Global evaluation of CCN formation by direct emission of sea salt and growth of ultrafine sea salt

Jeffrey R. Pierce[1] and Peter J. Adams[2,3]

Received 4 May 2005; revised 16 August 2005; accepted 7 December 2005; published 16 March 2006.

[1] The contribution of both the sea-salt emissions and specifically the ultrafine (dry $D_p < 0.1$ μm) component of these emissions to global CCN was assessed with a global model of aerosol microphysics. Four sea-salt emissions parameterizations were incorporated into the GISS II-prime general circulation model with the size-resolved aerosol microphysics module, TOMAS. The results of the four simulations were compared to observations of monthly average PM_{10} sea-salt mass, sea-salt mass size distributions, and marine aerosol number distributions. The agreement of the simulations with the observations varied greatly based on the sea-salt emissions parameterization used, but validation of the parameterizations is limited by uncertainty in the model's wind speeds. The impact of sea-salt aerosols on CCN concentrations was assessed by looking at the percent change in CCN(0.2%) concentrations between a simulation including both sea salt and sulfate and a simulation including sulfate alone. Two of the emissions parameterizations included ultrafine sea-salt particles, and the contribution of the ultrafine particles to CCN(0.2%) formation was assessed by sensitivity studies. Depending on the emissions estimate used, the addition of sea salt increased CCN(0.2%) over the Southern Ocean by 150% to 500%. The highest increases resulted from the simulations that included ultrafine emissions where it was found that the ultrafine sea salt can increase CCN(0.2%) concentrations over both the Southern Ocean and Antarctica by more than 50% relative to the same parameterizations with ultrafine sea salt excluded. The sensitivity of CCN(0.2%) to ultrafine sea-salt emissions enhances the importance of reducing the uncertainty of sea-salt emissions parameterizations and their subsequent treatment in aerosol models.

Citation: Pierce, J. R., and P. J. Adams (2006), Global evaluation of CCN formation by direct emission of sea salt and growth of ultrafine sea salt, *J. Geophys. Res.*, *111*, D06203, doi:10.1029/2005JD006186.

1. Introduction

[2] Anthropogenic emissions of aerosols and their precursors affect climate by scattering and absorbing solar and terrestrial radiation [*Angstrom*, 1929; *Charlson et al.*, 1992] and through the modification of the radiative properties and lifetimes of clouds [*Albrecht*, 1989; *Twomey*, 1974, 1977]. These two phenomena are known, respectively, as the direct and indirect effects of aerosols on climate. The indirect effect occurs when anthropogenic emissions of aerosols and aerosol precursor gases increase the number of cloud condensation nuclei (CCN) in the atmosphere. The increase in CCN causes a brightness effect by clouds reflecting more solar radiation and a lifetime effect by reduction of their precipitation efficiency. The magnitude of the global-average indirect radiative forcing on cloud brightness was assessed by the third Intergovernmental Panel on Climate Change to be between 0 and -2.0 W m^{-2} (cooling) with no best estimate [*IPCC*, 2001]. Unfortunately, they assessed the current scientific understanding of the aerosol indirect effect (both brightness and lifetime) as "very low". Many of these uncertainties result from nonlinear microphysical interactions between aerosols and aerosol precursor gases that determine CCN concentrations, such as coagulation, condensation and nucleation, along with poorly characterized spatial and temporal variations in CCN concentrations and uncertainties in cloud physics.

[3] Whether a particle is a CCN or not depends on the supersaturation of water vapor in the cloud along with the size and composition of the particle. Therefore, aerosol microphysical processes, such as coagulation, condensation of gases and aqueous oxidation of sulfur dioxide that influence the size and composition of the aerosols are factors controlling CCN concentrations. The first global models that quantified the indirect effect did not explicitly simulate changes in the aerosol composition and size distribution due to aerosol microphysics; rather, they used parameterizations based on bulk aerosol mass to estimate the change in cloud droplet number concentrations (CDNC)

[1]Department of Chemical Engineering, Carnegie Mellon University, Pittsburgh, Pennsylvania, USA.
[2]Department of Civil and Environmental Engineering, Carnegie Mellon University, Pittsburgh, Pennsylvania, USA.
[3]Department of Engineering and Public Policy, Carnegie Mellon University, Pittsburgh, Pennsylvania, USA.

0148-0227/06/2005JD006186

resulting from anthropogenic influence [*Boucher and Lohmann*, 1995; *Chuang and Penner*, 1995; *Chuang et al.*, 1997]. More recently, models have been developed that explicitly track the changes in the aerosol distribution by microphysical processes [*Adams and Seinfeld*, 2002; *Ghan et al.*, 2001; *Gong et al.*, 2003, 2002; *Herzog et al.*, 2004; *Rodriguez and Dabdub*, 2004; *Stier et al.*, 2005; *Vignati et al.*, 2004; *Wilson et al.*, 2001].

[4] Anthropogenic emissions of aerosols and aerosol precursor gases interact with natural aerosols causing increases in CCN concentration to be nonlinear with the addition of anthropogenic emissions. Therefore, natural aerosols and precursor gases must be understood and included in such models in order to determine accurately the changes in CCN resulting from anthropogenic emissions. For example, in an area where there is a strong source of natural particles with diameter greater than about 0.1 μm (e.g., sea salt or dust), oxidation products of anthropogenic aerosol precursor gases will condense mainly onto the natural particles that dominate the aerosol surface area. Ultrafine (dry $D_p < 0.1$ μm) anthropogenic primary aerosols will tend to coagulate with the larger existing aerosols before they can grow to CCN sizes, thus not greatly changing the CCN concentrations at typical ambient supersaturations. On the other hand, when there is not a strong source of natural particles, ultrafine anthropogenic particles are more likely to grow through condensation and coagulate with other ultrafine particles to grow to CCN sizes, thus having a greater impact on the CCN concentrations. Furthermore, it may be important to model properly the natural ultrafine emissions when assessing the aerosol indirect effect, because coagulation with anthropogenic ultrafine particles and condensation of anthropogenic gases may cause the natural ultrafine particles to grow to CCN sizes.

[5] Sea-salt aerosols, with mineral dust, comprise most of the natural aerosol mass [*Seinfeld and Pandis*, 1998]. Sea salt is a major source of CCN in remote marine areas and interacts with anthropogenic aerosols in polluted marine regions [*O'Dowd et al.*, 1997]. Sea-salt aerosols are generated by bubbles bursting at the surface of the ocean (film and jet drops) and by droplets being torn off of wave crests (spume drops) [*Andreas*, 1998; *Monahan et al.*, 1986]. Much effort has been expended recently towards developing methods to predict the emissions of sea salt. Data have been collected in both coastal and open-ocean field campaigns along with indoor bubble tanks for the development of parameterizations of sea-salt emissions. There is significant variability regarding the emissions flux and applicable particle size ranges between the various parameterizations. These parameterizations tend to agree within a factor of 4 for number fluxes [*Lewis and Schwartz*, 2004]. The uncertainty in sea-salt number fluxes adds to the uncertainty in the aerosol indirect effects [*Lewis and Schwartz*, 2004].

[6] Several authors have published size-resolved sea-salt emissions flux estimates from oceanic whitecaps [*Clarke et al.*, 2006; *Gong*, 2003; *Martensson et al.*, 2003; *Monahan et al.*, 1986; *Smith et al.*, 1993]. *Smith et al.* [1993] and *Clarke et al.* [2006] based their parameterizations on coastal observations, while *Martensson et al.* [2003] and *Monahan et al.* [1986] based theirs on measurements performed in indoor tanks. *Gong* [2003] modified the emissions parameterization in *Monahan et al.* [1986] to include a sub-micron emission spectrum of shape similar to the sub-micron concentration spectrum published in *O'Dowd et al.* [1997]. An alternative method to parameterize the emissions flux was used by *O'Dowd et al.* [1997], who presented a regression model of ambient sea-salt concentrations and size-distributions with wind speed using ship observations in the North Atlantic. In general, the number fluxes given by these parameterizations depend strongly on the conditions under which the sample data were collected and the sampling technique used, causing large discrepancies between emissions estimates.

[7] Until recently, sea-salt emissions with dry diameter smaller than 0.1 μm were not included in the emissions estimates. With improvements in measurement techniques and increased interest in understanding CCN concentrations, several recent parameterizations have included the distributions below 0.1 μm and shown significant sources of sea-salt number in this size range [*Martensson et al.*, 2003; *Clarke et al.*, 2006]. With a significant portion of the number flux in these parameterizations in the ultrafine (dry $D_p < 0.1$ μm) mode, these particles could make substantial contributions to CCN concentrations. Several global sea-salt aerosol modeling studies have been conducted [*Gong*, 2003; *Gong and Barrie*, 2003; *Gong et al.*, 2002; *Grini et al.*, 2002; *Guelle et al.*, 2001; *Liao et al.*, 2004]. While these studies have enhanced the understanding of the atmospheric burden and direct climate effect of sea-salt aerosols, none of these modeling studies included significant levels of ultrafine sea-salt emissions.

[8] This paper documents sea-salt model development in the TwO-Moment Aerosol Sectional (TOMAS) aerosol microphysics module currently run in the Goddard Institute for Space Studies General Circulation Model (GISS II-prime) [*Adams and Seinfeld*, 2002]. Four sea-salt emissions parameterizations are tested and associated model results are compared to observations. Evaluation of a CCN model requires observations other than total sea-salt mass because supermicron sea salt dominates sea-salt mass, whereas sub-micron sea-salt particles are much more efficient at contributing to CCN. Therefore, we will also compare our results with observations of sea-salt mass distributions and marine number distributions. For each of these parameterizations, we look at the ability of sea salt to enhance CCN concentrations in different global locations. We also use the model results to evaluate the impact of newly measured ultrafine sea-salt emissions on CCN concentrations. By using several sea-salt emissions estimates, we will explore the how the choice of sea-salt emissions parameterization adds uncertainty to cloud radiative forcings. This work is still limited in its ability to quantify the indirect effect of aerosols as it includes only sulfate and sea-salt aerosols. However, with sulfate and sea salt being the dominant species in remote marine regions [*O'Dowd et al.*, 1997], it should be adequate for evaluating CCN in these regions and provides a stepping stone in the development of the TOMAS aerosol microphysics module.

[9] The following section provides a description of the GISS II-prime general circulation model (GCM), TOMAS aerosol microphysics module, and the sea-salt parameterizations used along with a discussion on the uncertainties in wind speeds. The budget information from the simulations is presented in section 3. Section 4 compares the model

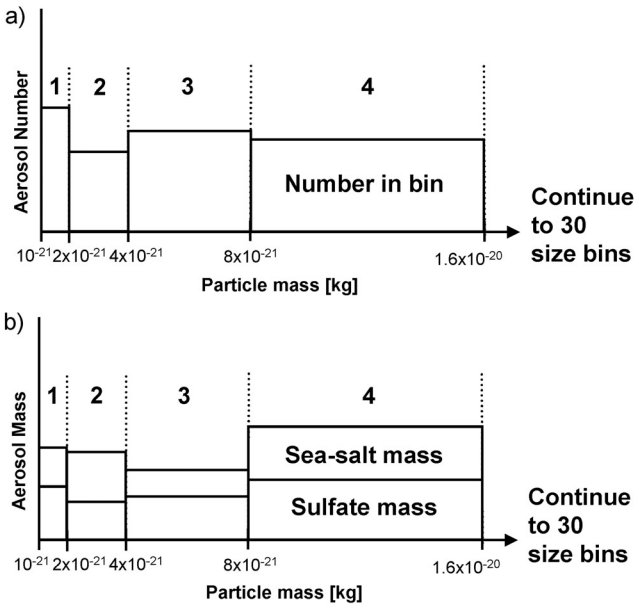

Figure 1. (a) Aerosol number distribution in TOMAS. (b) Aerosol mass distribution in TOMAS for sea-salt and sulfate model.

predictions to observations. The influence of sea salt generally on CCN concentrations along with the uncertainty in CCN concentrations based on the choice of sea-salt emissions estimate is presented in section 5. Section 6 looks at the impact of ultrafine sea salt on CCN concentrations, and the conclusions are presented in section 7.

2. Model Description

2.1. Overview

[10] The original version of the GISS GCM II was presented in *Hansen et al.* [1983], but many subsequent improvements have been made [*Del Genio and Yao*, 1992; *Del Genio et al.*, 1996; *Hartke and Rind*, 1997; *Prather*, 1986; *Rind and Lerner*, 1996]. The version of the model used in this paper has horizontal grid dimensions of 4° latitude and 5° longitude and nine vertical layers extending into the stratosphere to the 10 mb level. Sea-surface temperatures are specified based on climatological averages.

[11] Gas-phase H_2O_2, DMS, SO_2 and H_2SO_4, along with the aerosol number distribution, sulfate and sea-salt aerosol mass distributions and bulk MSA aerosol are all predicted variables in the model. The model sulfur chemistry was developed by *Koch et al.* [1999] and includes dimethyl sulfide (DMS) oxidation by OH to form SO_2 and MSA, DMS oxidation by NO_3 at night to form SO_2, gas phase oxidation of SO_2 by OH to form H_2SO_4, and liquid phase oxidation of SO_2 by H_2O_2 to form H_2SO_4. There has been no significant change made to the sulfur chemistry since *Koch et al.* [1999]. H_2O_2 is carried as a prognostic variable and is created through the HO_2 self reaction and destroyed photochemically by reaction with OH and reaction in the liquid phase with SO_2. The concentrations of OH and HO_2 and the photolysis rate of H_2O_2 are specified based on five-day averages. The DMS emissions are calculated using the sea-surface concentrations from *Kettle et al.* [1999] and the air-sea gas exchange parameterization of *Liss and Merlivat* [1986].

[12] The TwO-Moment Aerosol Sectional (TOMAS) microphysics model tracks the aerosol chemical composition and size distribution [*Adams and Seinfeld*, 2002, 2003; *Feingold et al.*, 1988; *Tzivion et al.*, 1987]. The advantage of the TOMAS algorithm and other two-moment sectional algorithms [e.g., *Jacobson*, 2002] is that it tracks two independent moments of the aerosol size distribution, the number and mass of aerosols within the GCM grid cell, for each size bin. This is beneficial because calculating the number and mass concentrations independently allows the average particle mass (mass in a size bin divided by the number in that size bin) within each bin to vary, whereas single moment methods require a fixed average particle mass. When the average particle mass within a size bin is fixed, one must chose between conserving the moment that is not explicitly tracked (number or mass depending on which one is being calculated) or preserving the shape of the distribution.

[13] Figure 1 shows how the aerosol size distributions are represented in TOMAS. The aerosol distribution is divided into 30 size bins defined by an individual particle's dry mass. The lower boundary of the smallest size bin is 10^{-21} kg dry mass, and each successive boundary doubles the mass of the previous boundary. The resulting size distribution spans 10 nm to 10 μm dry diameter for typical aerosol densities. We assume that particles are internally mixed; therefore, in each size bin the total number of particles is tracked along with the mass of sulfate and the mass of sea salt. With 30 predicted variables each for aerosol number, sulfate mass, sea-salt mass and aerosol water mass, 120 parameters are required to describe the aerosol size-composition distribution. Adding the four gaseous species and bulk MSA gives a total of 125 predicted variables.

[14] For the treatment of wet deposition and aqueous chemistry, convective clouds are assumed to have a supersaturation of 1.0% and large-scale clouds are assumed to have a supersaturation of 0.2%. For our sulfate/sea-salt aerosol model, we assume that all aerosols larger than 40 nm are activated in convective clouds and all aerosols larger than 80 nm are activated in large-scale clouds. The fraction of activated aerosols that wet deposit is proportional to the fraction of the cloud water that precipitates. All aerosols are subject to below-cloud scavenging. The size-resolved dry deposition rates are calculated using the resistance in series approach accounting for the size-dependent gravitational settling of particles and a size-dependent resistance in the quasi-laminar sublayer [*Seinfeld and Pandis*, 1998]. Further discussion on sulfate aerosol sources, aerosol sinks and aerosol microphysics is included in *Adams and Seinfeld* [2002].

[15] The aerosol nucleation parameterization used in the model is a simple binary (H_2SO_4 and H_2O) nucleation parameterization [*Adams and Seinfeld*, 2002]. For reasons discussed in *Adams and Seinfeld* [2002], this may underpredict nucleation rates. Moreover, it has been reported in *Clarke et al.* [1998] that binary nucleation predicts no nucleation in typical marine boundary layer conditions and other theories must be used. To the extent that the model does underpredict new particle formation in the

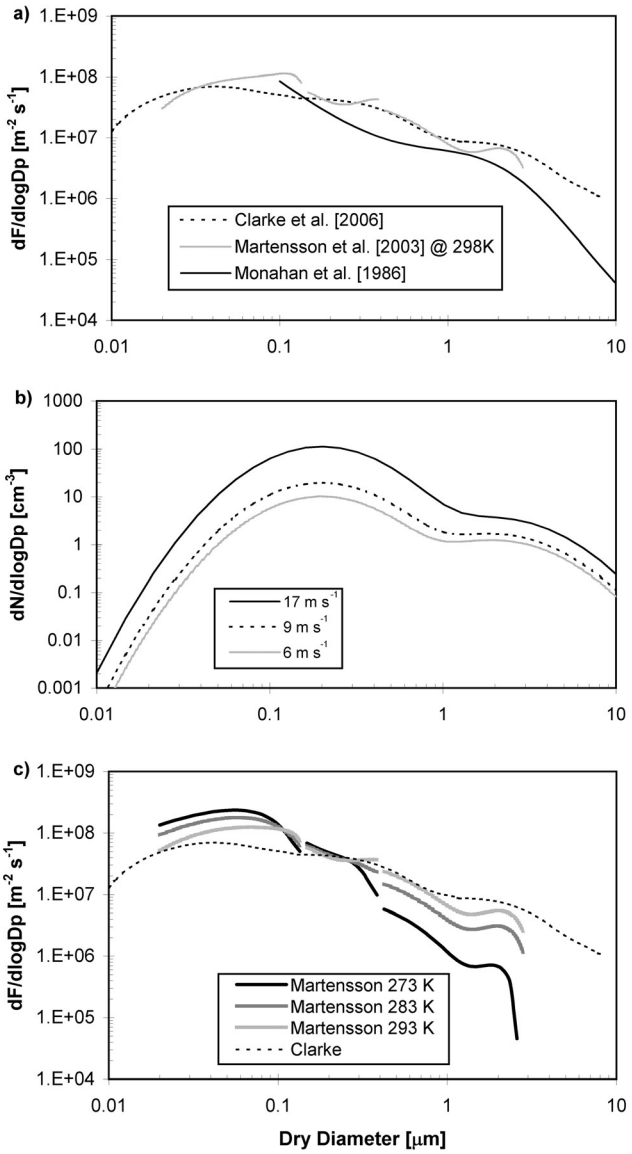

Figure 2. (a) Sea-salt number flux from per unit whitecap area for Clarke, Martensson(298 K) and Monahan parameterizations. Discontinuities in the Martensson source function stem from breaks between their three polynomial fits. (b) The sea-salt number distribution above ocean for three wind speeds using the O'Dowd parameterization. (c) Number emissions flux of the Martensson and Clarke (not temperature dependent) emissions parameterizations per whitecap area at three temperatures.

marine boundary layer, it may overestimate the relative importance of sea-salt emissions to CCN concentrations.

[16] The internal mixing assumption used in this model unrealistically mixes sulfate and sea salt instantaneously within a given size bin into the same particles. However, since the main goal of this study is to evaluate sea-salt effects on CCN and both sea-salt and sulfate aerosols activate at similar diameters (~80 nm for 0.2% supersaturation), the effect of this instantaneous internal mixing should be small. In other words, when a sea-salt aerosol is emitted into a size bin in the surface layer, it will not greatly matter in our CCN calculations whether that particle is pure sea salt or a sea-salt/sulfate mixture as long as the sizes and numbers of the particles are preserved.

2.2. Sea-Salt Emissions Parameterizations

[17] Four sea-salt emissions parameterizations are used in this study. The size distributions of the various emissions parameterizations are shown in Figure 2. They are described in Table 1 with the names of their associated simulations. A control run (SULF) simulates sulfate aerosol but no sea salt. The SULF simulation is the same as the "primary emissions" simulation in *Adams and Seinfeld* [2002]. The CLRK run uses the emissions estimate derived from a coastal field campaign to find the sea-salt number flux and fit the size distribution of the emissions flux to polynomials spanning dry diameters of 10 nm to 8 μm [*Clarke et al.*, 2006] (Figure 2a). The MART run uses emissions parameters developed by *Martensson et al.* [2003] from measurements of whitecaps generated in a bubble chamber (Figure 2a). Their size-resolved number flux as a function of diameter was expressed as polynomials from 20 nm to 2.8 μm dry diameter. A unique feature of this parameterization is that the size distribution and magnitude of the emissions flux vary with temperature (Figure 2c). The emissions of ultrafine (dry $D_p < 0.1$ μm) particles are greatly increased and the emissions of coarse particles are greatly reduced in low temperature water. The CL100 and MA100 runs are the same as the CLRK and MART runs, respectively, but omit emissions of sea-salt particles smaller than 100 nm dry diameter. The MON run uses emissions from *Monahan et al.* [1986], which is probably the most commonly used sea-salt emissions estimate in global aerosol models (Figure 2a). It is based on measurements of super-micron aerosol, but it has compared well to observations in previous modeling studies for number and mass concentrations when extrapolated to dry diameters of 0.1 μm [*Gong et al.*, 1997]. Only the film and jet drop equation given in *Monahan et al.* [1986] is used here because the larger spume mode does not contribute significantly to aerosol number concentrations. To obtain the sea-salt number flux from the ocean, the sea-salt number flux per whitecap area in these parameterizations is multiplied by the ocean area covered by whitecaps. The fractional area of the ocean covered by whitecaps is assumed to be that given by *Monahan and O'Muircheartaigh* [1980]:

$$W(U) = 3.84\left(10^{-6}\right)U_{10}^{3.41} \quad (1)$$

W is the fraction of the ocean covered by whitecaps and U_{10} is the wind speed 10 m above the ocean surface, given in m s^{-1}. This whitecap/wind correlation has been shown to give reasonable wind dependence of the sea-salt surface concentration when used in the *Monahan et al.* [1986] parameterization within the *Gong et al.* [1997] host model. There may, however, be variation in the sea-salt concentration dependence on wind speed between different models due to differences in model meteorology and deposition processes. The OD run uses the sea-salt estimate given in *O'Dowd et al.* [1997], where the number concentration of sea-salt aerosols near the ocean surface is given as a function of diameter and wind speed for three lognormal modes. This differs from the previous

Table 1. Overview of Simulations[a]

Name	Description	Smallest Sea-Salt Particle Emitted	Largest Sea-Salt Particle Emitted	Emissions Reference
SULF	Aerosol sulfate only	N/A	N/A	*Adams and Seinfeld* [2002]
CLRK	Clarke sea-salt emissions	10 nm	8 μm	*Clarke et al.* [2006]
CL100	Same as CLRK but no sea salt emitted smaller than 100 nm	100 nm	8 μm	*Clarke et al.* [2006]
MART	Martensson sea-salt emissions	20 nm	2.8 μm	*Martensson et al.* [2003]
MA100	Same as MART but no sea salt emitted smaller than 100 nm	100 nm	2.8 μm	*Martensson et al.* [2003]
OD	O'Dowd sea-salt emissions	100 nm[b]	10 μm	*O'Dowd et al.* [1997]
MON	Monahan sea-salt emissions	100 nm	10 μm	*Monahan et al.* [1986]

[a]All simulations include sulfate. Sea-salt size cutoffs are dry diameter.
[b]The method of *O'Dowd et al.* [1997] gives the number concentration of sea-salt particles in the marine boundary layer as a function of wind speed in two lognormal modes. The number of particles smaller than 100 nm is negligible.

estimates in that the concentration is specified rather than the emissions flux. *O'Dowd et al.* [1997] measured aerosols to sizes as small as D_p = 0.1 μm dry diameter. The lognormal fits in their parameterization extended to aerosols smaller than this, but the number of ultrafine aerosols predicted by the parameterization is very small and not based on measurements. Because of this, the OD parameterization will not be used to explore the impact of ultrafine sea salt on CCN concentrations. Figure 2b shows the size-resolved sea-salt number concentration above the ocean at 10 m wind speeds of 6, 9 and 17 m s^{-1} for the *O'Dowd et al.* [1997] parameterization. To apply this parameterization to our model, we specify that, if the concentration of sea salt within the grid cell and size bin is less than the value predicted by *O'Dowd et al.* [1997], the model concentration is increased to the predicted level. If the model concentration is higher than that predicted by the parameterization, we leave the model concentration the same. This method of applying the *O'Dowd et al.* [1997] parameterization to the entire surface layer of the model (approximately 400 m thick) may cause an overestimation of sea-salt concentrations as it does not account for a sea-salt concentration gradient between the ship observation level and higher levels of the first model layer. This would, in particular, affect the coarse mode sea salt that has higher dry deposition velocities.

2.3. Sea-Salt Emission Uncertainty Due to Bias in Wind Speed

[18] Incorrect mean wind speeds and wind speed distributions in the model can lead to large errors in sea-salt emissions. For the emissions estimates used in the CLRK, MART and MON model runs, the sea-salt emissions are proportional to $U_{10}^{3.41}$, where U_{10} is the wind speed 10 m above the ocean surface. The strong dependence means that errors in wind speed are magnified to larger errors in sea-salt emissions. Also, increased variability of wind speed about the mean leads to greater sea-salt emissions, so an overprediction (underprediction) of variability may also lead to an overprediction (underprediction) of sea-salt emissions.

[19] We have assessed our model's time-averaged sea-salt emissions potential ($U_{10}^{3.41}$) by comparing the average sea-salt emissions potential of the model to that of the National Center for Environmental Prediction (NCEP) reanalysis of U_{10} wind fields for the years 1996–2000. The advantage of using the sea-salt emissions potential rather than simply U_{10} is that the model bias in the emissions potential is equal to the model bias in sea-salt emissions. Figure 3 shows the seasonally averaged sea-salt emissions potential bias of the model when compared to the NCEP reanalysis product. A value of positive four corresponds to a model overprediction by a factor of four, whereas a value of 0.25 corresponds to a model underprediction by a factor of four. In all seasons in Figure 3, the sea-salt emissions potential for the model underpredicts sea-salt emissions compared to NCEP throughout much of the ocean. In particular, with the exception of the eastern Pacific Ocean, the model tends to underpredict sea-salt emission in the tropical region. Also shown at the top of each plot is the globally averaged sea-salt emissions potential ratio, which is the ratio of sea-salt emissions using the GISS model winds versus the emissions using NCEP. This shows that on average, the model underpredicts sea-salt emissions by about 30–40% compared to NCEP. If the variability of the two wind sets are similar, this error corresponds to a difference in mean wind speed of about 10%, showing how strongly wind speed errors bias sea-salt emissions. With the assumption that the NCEP winds over the oceans are reasonably correct, the assessment above leads us to believe that for the specified spatial and time resolution of the model, the model winds are underpredicting the amount of sea salt emitted globally. Throughout the rest of this paper we will compare our model's predicted sea-salt concentrations to observations and evaluate the impact of sea salt on CCN concentrations in the marine boundary layer noting where the sea-salt emissions underprediction may affect the conclusions.

[20] Another problem with wind speeds in a GCM is that there is considerable uncertainty in the variability of the winds within the large GCM grid cells and also within the GCM's long time-steps. The artificial smoothing of the ocean surface wind variability will lead to some degree of sea-salt emission underprediction. *Cakmur et al.* [2004] explored a similar issue with dust emissions by using the GCM's boundary layer, dry convection and moist convection parameterizations to determine the sub-grid scale variations in wind speed. However, this issue has not yet been explored systematically for sea-salt emissions. Depending on the breadth of the distribution of winds

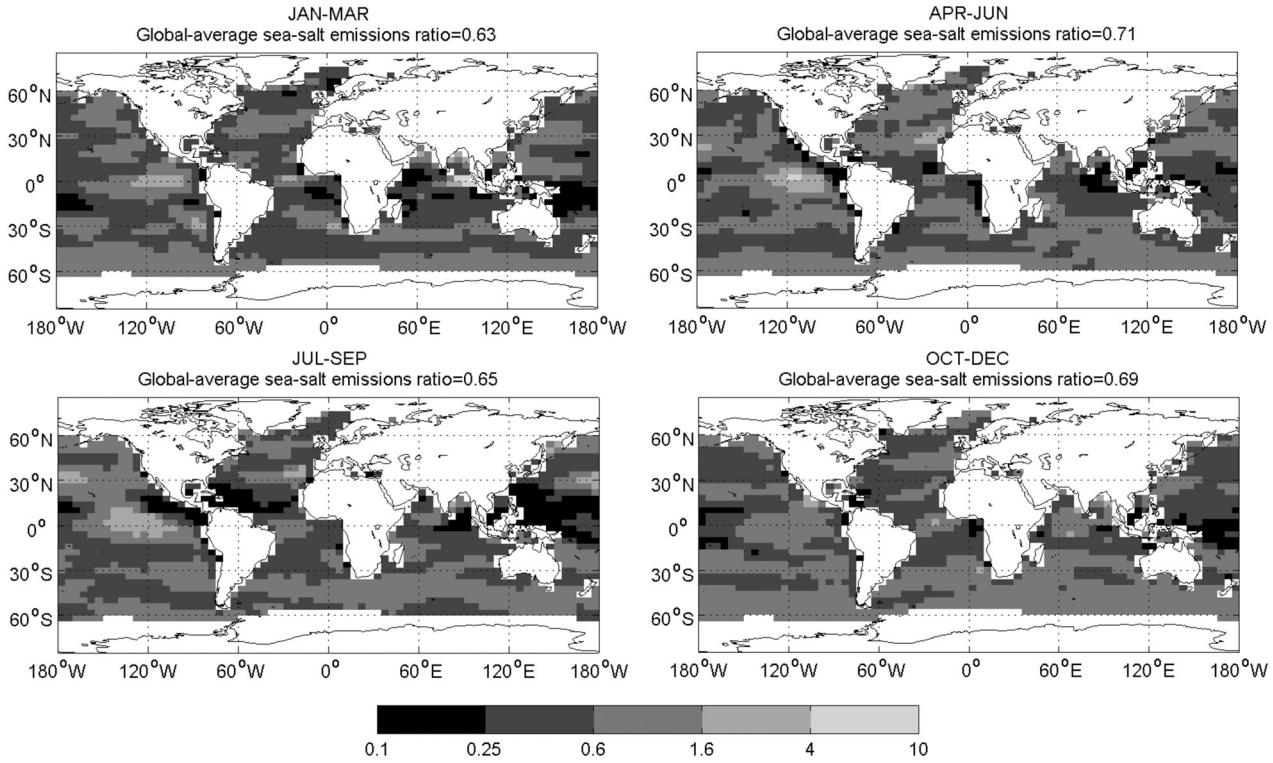

Figure 3. Ratio of seasonally averaged sea-salt emissions potential ($U_{10}^{3.41}$) in the GISS model to that from the NCEP reanalysis. This parameter directly corresponds to the ratio of emissions using the GISS and NCEP winds for the CLRK, MART and MON runs. The global-average sea-salt emissions ratio is area-weighted avg($U_{10}^{3.41}{}_{\mathrm{GISS}}$)/avg($U_{10}^{3.41}{}_{\mathrm{NCEP}}$) of all open-ocean during the corresponding time period.

within the grid cell and time-step, the model may be further underestimating the sea-salt emissions.

3. Global Budget Information

[21] Annually and globally averaged sea-salt budget information from simulations using the four emissions parameterizations is given in Table 2. The burden, sources and sinks for each simulation are broken up into sub-micron and super-micron dry diameter amounts. The budget information for the CL100 and MA100 runs are not shown because omission of the sub-100 nm particles does not greatly change the sub-micron mass budget. The budget information is for intercomparison between models and parameterizations and should not be taken as estimates for the total global sea-salt mass budgets. This is because the emissions parameterizations have arbitrary upper diameter limits, and we do not take into account the spume mode aerosols, neither of which greatly affects CCN concentrations at the fixed supersaturations we have explored in this paper. However, these large aerosols may act as giant CCN (GCCN). GCCN may alter the cloud microphysics and may lower the maximum supersaturation of the cloud [*Feingold et al.*, 1999].

[22] The sources and burdens greatly depend on the emissions parameterization. The super-micron burden differs by a factor of 10 between the CLRK and MART parameterizations. This results from the CLRK parameterization maintaining a high number flux in the super-micron range and the MART parameterization having an upper limit dry diameter of 2.8 μm. The sub-micron sources and burden differ between the CLRK and OD parameterizations by more than a factor of 2.5. The sub-micron lifetime varies by less than 25% between simulations with different parameterizations. The super-micron lifetime varies somewhat depending on the average particle mass of emissions. For example, many super-micron particles of the OD parameterization are emitted close to 10 μm dry diameter where

Table 2. Sea-Salt Aerosol Budget Information From Four Model Simulations

	Burden, Tg	Sources, Tg yr^{-1}	Wet Deposition, Tg yr^{-1}	Dry Deposition, Tg yr^{-1}	Lifetime, Days
CLRK < 1 μm	0.73	98.1	90.5	7.6	2.72
CLRK > 1 μm	12.2	7020	2070	4950	0.64
MART < 1 μm	0.42	64.9	61.5	3.3	2.35
MART > 1 μm	1.38	494	290	204	1.02
OD < 1 μm	0.29	49.1	46.3	2.8	2.16
OD > 1 μm	16.7	13200	3800	9440	0.46
MON < 1 μm	0.37	51.0	46.6	4.5	2.67
MON > 1 μm	3.48	1710	573	1140	0.74

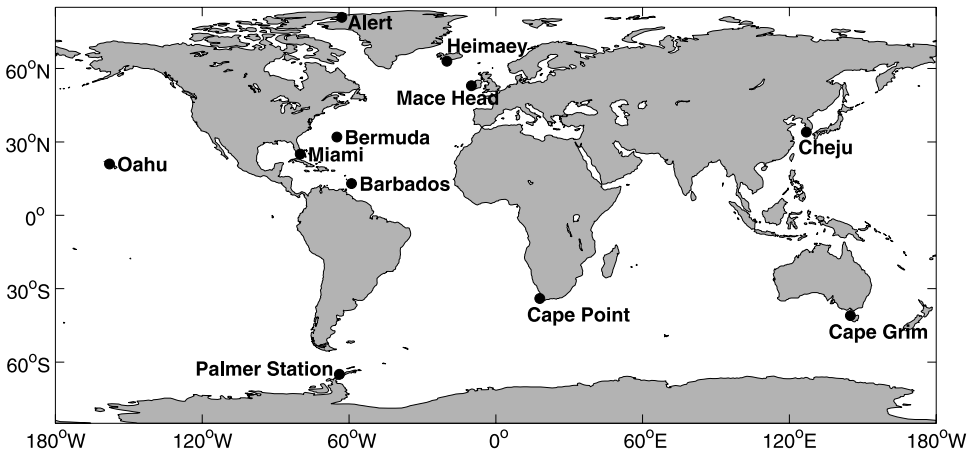

Figure 4. Locations for total sea-salt mass comparison with observations.

dry deposition velocities are high, giving it a lower lifetime than the super-micron particles in the MART parameterization that are all emitted below 2.8 μm.

[23] *Guelle et al.* [2001] published global sea-salt mass burden information using the *Monahan et al.* [1986] source parameterization. They found the sub-micron burden to be 0.15 Tg, slightly less than half of our estimate. Their burden between 1 μm < D_p < 8 μm was 3.1 Tg, nearly matching our estimate. On the other hand, *Gong et al.* [2002] published global source information for sub-micron sea salt using the *Monahan et al.* [1986] parameterization and they found the total source to be 180 Tg yr^{-1}, about 3.5 times larger than our source term. The low bias of sea-salt emissions in our model due to the underprediction of $U_{10}^{3.41}$ accounts for about 20% of this difference. An additional difference may be that *Gong et al.* [2002] scaled their U_{10} by a constant factor to match the mean wind speed of the European Centre for Medium-Range Weather Forecasting (ECMWF) mean U_{10} wind speed. This constant scaling does not take into account spatial and temporal variability, thus not necessarily predicting the same sea-salt emissions as the ECMWF wind fields. If the model used in *Gong et al.* [2002] has a high variability of wind speeds, this could account for more of the discrepancy between the model emissions. This shows how important model processes other than the emissions parameterization can be and cautions against concluding that an emissions parameterization is superior to another based on comparison of chemical transport model results to observations.

[24] The burden, lifetime, sources and sinks for DMS, SO_2 and SO_4^{2-} are similar for all model runs to those published by *Adams and Seinfeld* [2002] and *Koch et al.* [1999]. The annual-average global burden of SO_4^{2-} is 0.77 Tg S and the lifetime is 6.2 days. The reduction in lifetime compared to 6.6 days for the sulfate-only model [*Adams and Seinfeld*, 2002] is due to condensation of sulfate onto CCN sized primary sea-salt particles reducing the wet-deposition lifetime and condensation of sulfate onto coarse mode sea-salt particles reducing the dry deposition lifetime.

4. Comparisons to Observations

4.1. Monthly Sea-Salt Mass Concentrations

[25] The sites chosen for comparison of the seasonal cycle of sea-salt mass are part of a network of coastal sites that monitor aerosol compositions [*Savoie and Prospero*, 1977]. Sites were chosen from the available dataset to include a variety of meteorological conditions and varying amounts of anthropogenic influence. Figure 4 shows these chosen locations. For our comparison, we omitted predicted sea-salt mass associated with particles larger than 4 μm dry diameter to attempt to match the PM_{10} inlet of typical aerosol samplers in an environment with ~80% relative humidity, similar to the procedure used by *Guelle et al.* [2001]. Small variations in this cutoff diameter greatly affect the CLRK and OD results because a large amount of their sea-salt mass emissions are near to or greater than 4 μm dry diameter.

[26] Figure 5 shows the comparison of the sea-salt mass concentrations from the four simulations with observational data at the eleven locations. Table 3 shows the mean normalized biased (MNB) and the mean absolute normalized gross error (MANGE) for each of the model runs. In general, the OD and CLRK simulations agree best with the observations having the smallest biases and the lowest error. The MART and MON results underpredict the sea-salt mass concentrations by factors of 3 to 4. This is because the MART and MON parameterizations predict lower emissions than the CLRK and OD emissions in super-micron sizes with no MART emissions larger 2.8 μm (see Figure 2). Generally, the sea-salt mass concentration predicted in the MON simulation is smaller than the mass predicted by model runs using the *Monahan et al.* [1986] emissions flux parameterization in similar sea-salt modeling studies [*Gong et al.*, 2002; *Guelle et al.*, 2001]. In the host models used in those studies, the *Monahan et al.* [1986] parameterization yielded results in better agreement with the same observations. The underprediction of sea-salt emissions due to bias in our model wind speeds may account for some of this error. This would also cause the CLRK and OD model runs to overpredict the sea-salt concentrations in many locations. It is difficult to say definitively which parameterization is best because of errors in both the model meteorology and treatment of aerosol processing, along with uncertainties in observational data.

[27] In general, the emissions flux based methods (CLRK, MART, MON) tend to have greater seasonal variability than the OD run. These cycles sometimes follow the trends of the observational data (Bermuda, Heimaey,

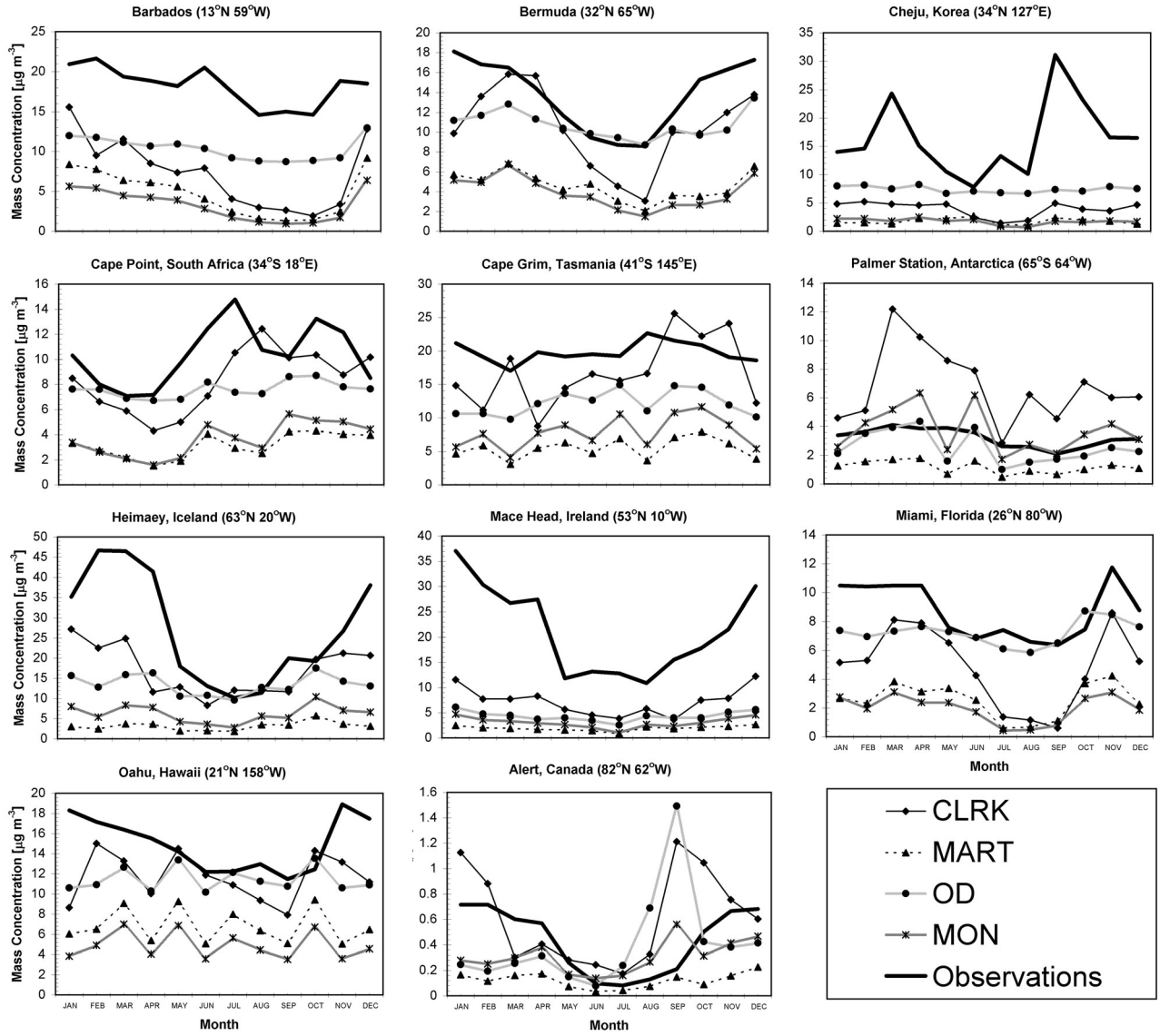

Figure 5. Total sea-salt aerosol mass concentrations [$\mu g\ m^{-3}$ at 273 K and 1 atm] from four simulations and observations at several locations.

Mace Head, Miami) but deviate from these trends in other cases (Cape Grim, Palmer Station, Oahu). The lower seasonal variability of the OD run is most likely the result of a lower dependence on wind speed than the emissions flux based methods. Increasing wind speed from 6 m s^{-1} to 9 m s^{-1} increases the number emissions flux for the CLRK, MART and MON runs by about 300%, whereas the OD parameterization shows only a 50% increase in the sea-salt number concentration. The change of emissions and concentrations are not directly comparable because of changes in deposition velocity and vertical mixing at higher wind speeds, but the weaker dependence of sea-salt number concentration on wind speed for the OD simulation is consistent with Figure 5.

4.2. Sea-Salt Mass Size Distributions

[28] Because super-micron aerosol accounts for most of the sea-salt mass while sub-micron aerosol accounts for most of the CCN, total mass measurements do not give much information on whether a parameterization will predict the correct CCN concentrations. To assess how well the different emissions parameterizations predict the sea-salt size distribution, we compared our simulated sea-salt mass distributions to two sets of impactor data. *Quinn and Coffman* [1999] used a seven-stage Berner-type cascade impactor to measure sodium concentrations from which they deduced sea-salt mass concentrations. Presented in their paper is a collection of impactor data from five field campaigns broken

Table 3. Mean Normalized Bias and Mean Error in Total Sea-Salt Mass Concentrations From Each Simulation

Run	Mean Normalized Bias	Mean Absolute Normalized Gross Error
CLRK	−15%	54%
MART	−73%	73%
OD	−25%	45%
MON	−59%	69%

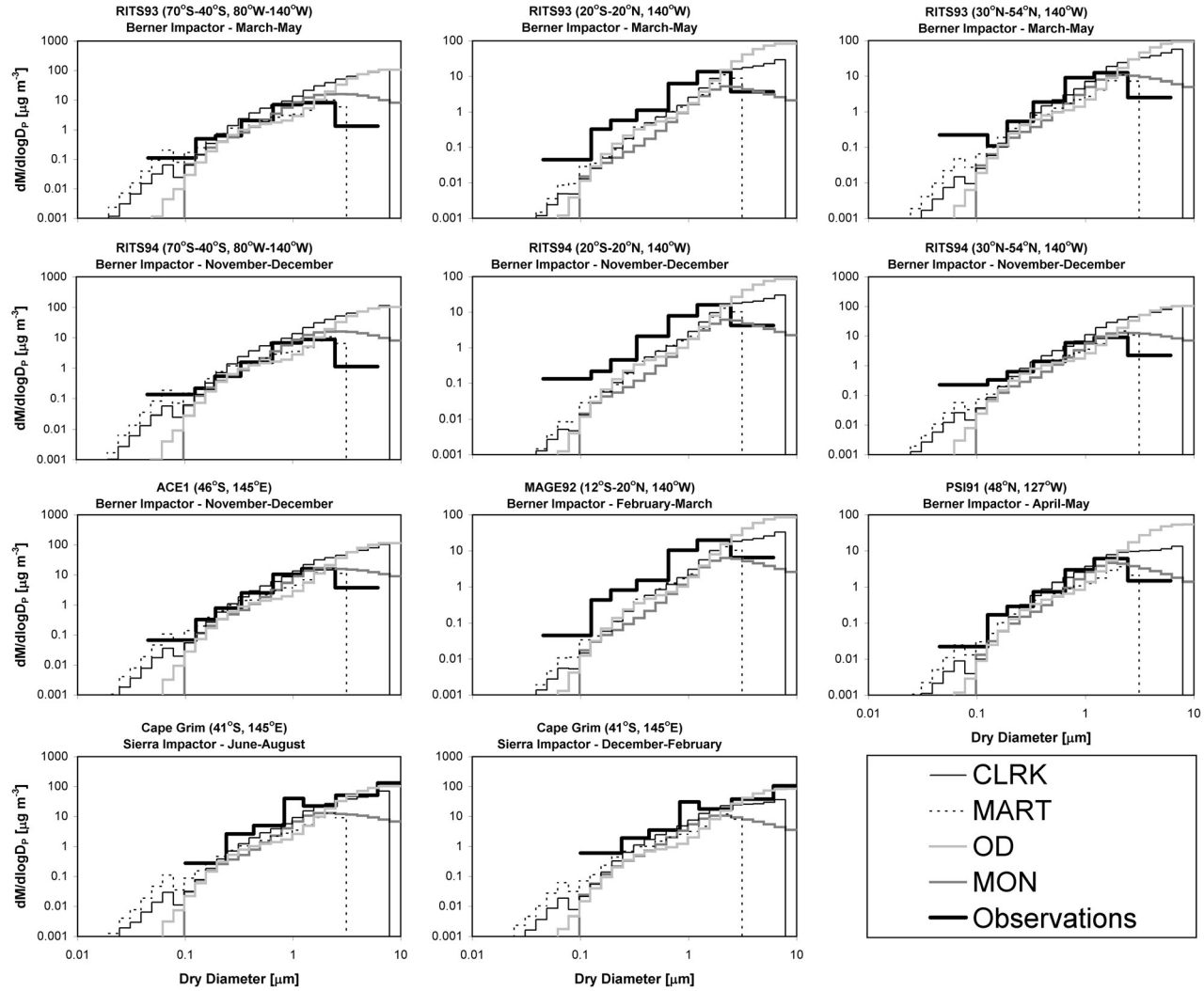

Figure 6. Sea-salt mass distributions at 273 K and 1 atm from simulations compared to observations from several marine locations and field campaigns. The upper nine panels are taken from *Quinn and Coffman* [1999], while the lower two are taken from *Andreae et al.* [1999].

into nine total categories by location and time of year. *Andreae et al.* [1999] used a seven stage Sierra-type cascade impactor. This data were collected at Cape Grim, Tasmania and includes observations from both summer and winter.

[29] Figure 6 shows predicted sea-salt mass size distributions with observational data for the eleven data categories discussed above and the average overprediction or underprediction of the simulation results for each impactor stage is shown in Figure 7. *Howell et al.* [1998] discussed performance differences between Berner and Sierra impactors and showed that Sierra impactors collected supermicron sea salt more effectively than the Berner impactor. This is noticeable in Figure 6 as the mass size distribution for the Berner impactor decreases above 2.5 μm dry diameter for all nine data sets, whereas it continues to rise for the Sierra impactor data in this size range.

[30] In mid to high latitudes, all four model runs have their best agreement with the Berner impactor distributions for sizes between 0.1 μm and 1 μm dry diameter. In tropical regions, all parameterizations yield much lower concentrations than those observed by *Quinn and Coffman* [1999]. The sea-salt mass observed by *Quinn and Coffman* [1999] in these tropical regions is actually somewhat higher than their observations in mid to high latitudes despite generally lower wind speeds in tropical regions. They believed that other factors, such as advection and vertical mixing, were also important in determining the sea-salt concentrations. The sea-salt aerosols may have had longer residence times in the area close to the ocean surface due to reduced vertical mixing, causing the concentrations of sea salt to be higher. However, as shown in Figure 3, the model, in general, greatly underpredicts the sea-salt emissions potential in tropical regions. This would account for some of this discrepancy.

[31] In Figure 7, the y-axis values are given as the log of the ratio of the predicted mass to the observed mass; a value of 0.5 means that, on average, the model overpredicted the mass on that impactor stage by $10^{0.5}$ or 3.2. This analysis shows again that the CLRK parameterization performed

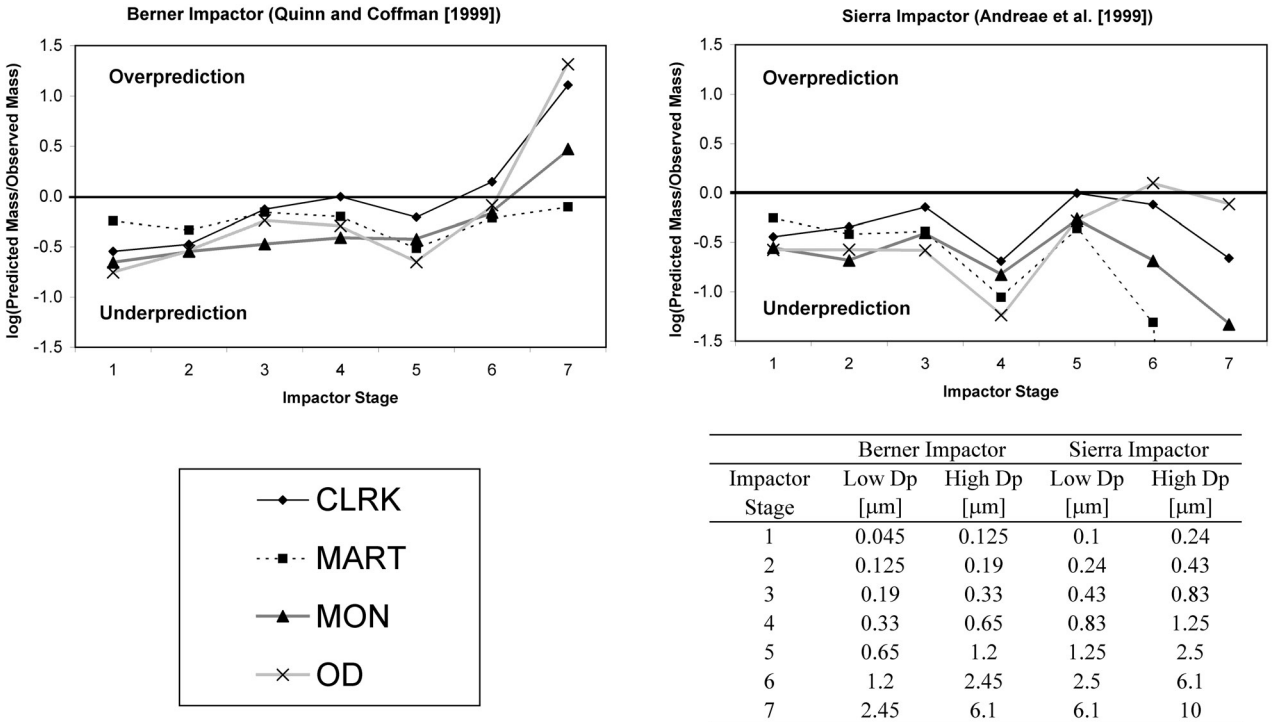

	Berner Impactor		Sierra Impactor	
Impactor Stage	Low Dp [μm]	High Dp [μm]	Low Dp [μm]	High Dp [μm]
1	0.045	0.125	0.1	0.24
2	0.125	0.19	0.24	0.43
3	0.19	0.33	0.43	0.83
4	0.33	0.65	0.83	1.25
5	0.65	1.2	1.25	2.5
6	1.2	2.45	2.5	6.1
7	2.45	6.1	6.1	10

Figure 7. Log of the ratio of the predicted mass concentrations to the observed mass concentrations for the four model simulations compared with each stage of the two impactors (Figure 5). A value of 0.5 corresponds to an overprediction by a factor of $10^{0.5}$ or 3.2. The sizes range for each stage of the two impactors is shown in the table.

best with the exception the smallest stages of both impactors and the largest Berner impactor stage, where *Howell et al.* [1998] claimed that the Berner impactor is inefficient in collecting aerosol mass. The MART parameterization appears to match observations fairly well for this stage, but its emissions only go up to 2.8 μm, whereas the stage collects particles with dry diameters from 2.45 to 6.1 μm. The errors associated with this stage are not greatly important when determining CCN because the number of aerosols associated with this size range is small; however, it is important to note that large sea-salt particles may act as giant CCN (GCCN) and initiate drizzle formation in stratocumulus clouds affecting the optical properties of the cloud [*Feingold et al.*, 1999]. The relatively complex effects of these GCCN will not be considered in this first-order exploration of sea salt and CCN.

[32] Unfortunately, impactor cutoffs and low resolution around 0.1 μm dry diameter do not give us any comparison for sea-salt aerosols smaller than 0.1 μm, where very high number emissions occur in the CLRK and MART simulations (see Figure 2). In general, more than half of CCN(0.2%) have sizes between 80 and 150 nm.

4.3. Marine Aerosol Number Distribution

[33] *Heintzenberg et al.* [2000] collected a large set of observations of marine aerosol size distributions and summarized them by fitting the aerosol number distributions to two lognormal modes for different latitudinal zones. The data used came from a wide array of sampling sites and field campaigns and used many different sampling instruments. The latitudinal bands are 15° wide with no data between 75°S–90°S and 60°N–75°N. The 15° by 15° grid cells from which the data were obtained is published in their paper (their Figure 1). Rather than using all ocean grid cells for comparison, we generally used model results from these same 15° by 15° sections where observations were collected. However, some of the 15° by 15° grid areas include continental areas (e.g. observations from Mace Head, Ireland are in the same 15° by 15° grid cell as most of the British Isles). Because the GCM grid resolution is finer, we exclude these continental sub-areas from our comparison as they greatly increase ultrafine number concentrations.

[34] Figure 8 shows the aerosol number distribution for the five model simulations (including the SULF run) and the two-modal fits published by *Heintzenberg et al.* [2000] for each of the latitudinal bands. The bimodal structure of the *Heintzenberg et al.* [2000] data is captured by the model. The critical diameter for aerosol activation in large-scale stratus clouds is assumed to be ~0.08 μm in our model, which explains why this is where the accumulation mode begins for all latitudes. The critical diameter for activation in the model in convective clouds is assumed to be ~0.04 μm dry diameter. This causes three modes to appear in the tropical and southern mid-latitude distributions. The severity of the cutoff between modes (e.g. in higher latitudes) is an artifact of our assumption of a single supersaturation for each cloud type, regardless of aerosol distribution and cloud thermodynamics, rather than a distribution of supersaturations. Elaboration of the supersaturation distribution is left for future work.

[35] All of the latitudinal bands between 90°N and 45°S showed a dominant influence of sulfate, which is shown by

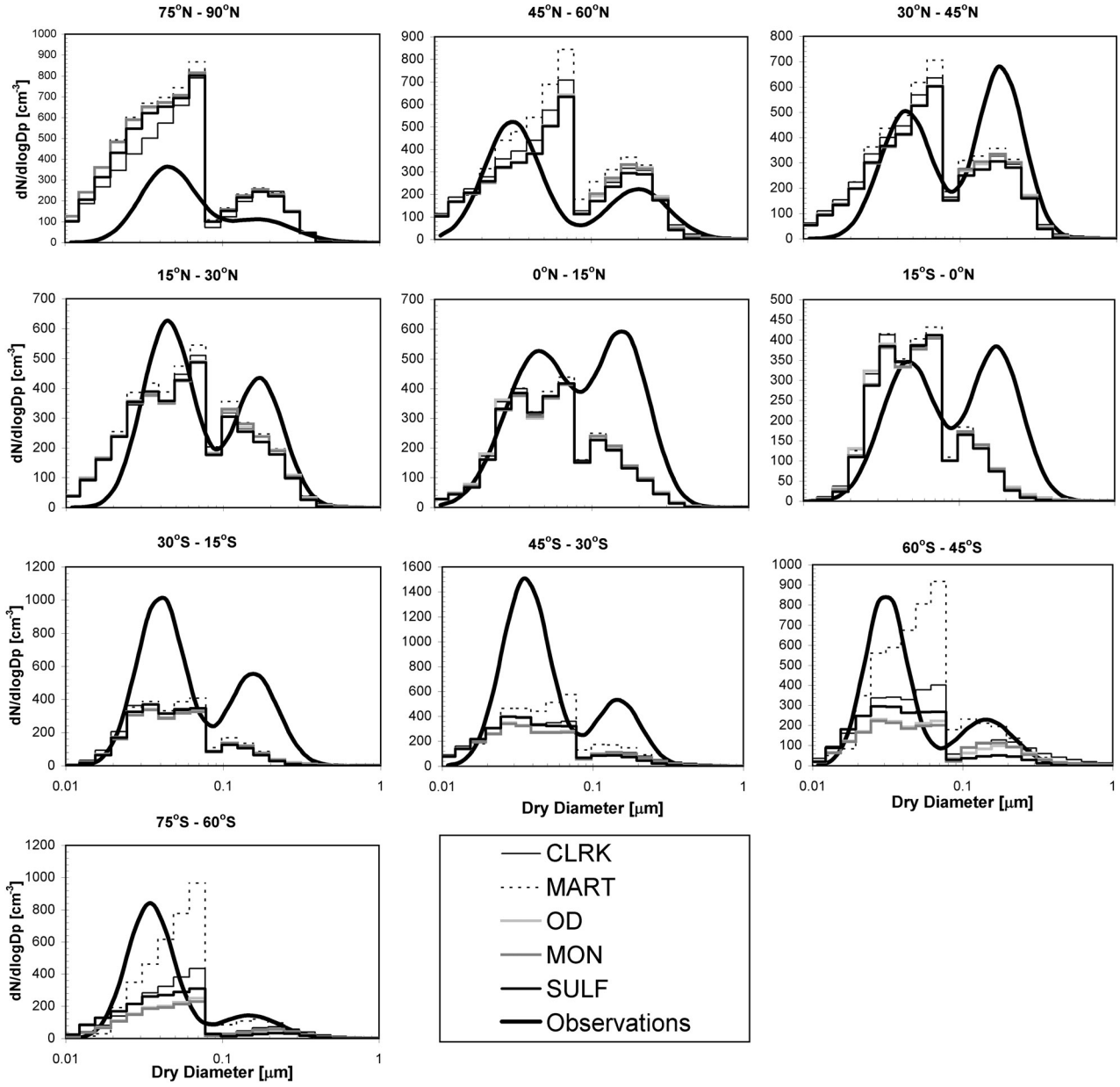

Figure 8. Comparison of marine aerosol number (sulfate and sea salt) distributions at 273 K and 1 atm published in *Heintzenberg et al.* [2000] with the four sea-salt simulations and the sulfate-only simulation. The grid cell locations chosen for the comparison represent the marine areas used to compile the *Heintzenberg et al.* [2000] data.

the number distribution of the sea-salt simulations nearly matching the SULF result. The model tends to overpredict number concentrations in the high northern latitudes, which may be because of an overprediction of continental influence. In the northern mid-latitude and tropical regions, the model predicts the ultrafine mode well but underpredicts the accumulation mode. The model underpredicts both modes between 15°S and 45°S, which may result from organics and dust not being treated in the GCM or a possible underprediction of sea-salt emissions in low latitude areas, which is consistent with the analysis in section 2.3.

[36] The largest differences between the various sea-salt parameterizations are apparent over the Southern Ocean (45°S to 60°S and the 60°S to 75°S) where the influence of anthropogenic sulfate is minimal. The impact of the ultrafine emissions of the CLRK and MART parameterizations (see Figure 2) is apparent in these latitude bands allowing their ultrafine number to match more closely that of the observations than the SULF simulation. Note that the number of ultrafine particles is lower in the OD and MON results than the SULF simulation. This is because the larger sea-salt particles provide a surface onto which sulfate condenses and ultrafine particles coagulate with, thereby suppressing nucleation in free troposphere and lowering ultrafine concentrations.

[37] Table 4 shows the mean normalized bias of the total number of particles in the ultrafine and accumulation modes

Table 4. Mean Normalized Bias of the Predicted Total Number of Particles in the Two Modes in the 45°S to 75°S Latitude Band for the Four Simulations Compared to the Observations in *Heintzenberg et al.* [2000]

	Size Range Dry Diameter, μm	CLRK	MART	MON	OD
Ultrafine	0.01–0.1	−39%	10%	−62%	−60%
Accumulation	0.1–1.0	−36%	−13%	−52%	−59%

in the 45°S to 75°S latitude band for the four sea-salt simulations compared to the observations of *Heintzenberg et al.* [2000]. These two latitudinal bands were chosen for this comparison because of the minimal influence of errors in the simulation of sulfate. The MART results are closest to predicting the number of both modes followed by the CLRK simulation. Both the OD and MON simulations underpredict both modes by a factor of two. These results suggest that the ultrafine emissions included in the CLRK and MART model runs may be necessary to reproduce observed ultrafine concentrations in these remote oceanic areas. However, uncertainties in the sources of ultrafine sulfate, including nucleation, make it unclear if this is definitely the case.

5. Sea Salt and CCN

[38] To look at the impact of sea-salt emissions on CCN concentrations, we compare CCN(0.2%) with and without sea-salt aerosols in the lowest layer of the model (Figures 9a and 9b). Only the lowest layer (∼400 m) is used because the second layer (up to ∼1.2 km) frequently extends into the marine free troposphere, thus not giving a clear picture of the aerosols in the marine stratus deck. For simplicity, we assumed that all aerosols larger than 80 nm will be activated in a cloud of 0.2% supersaturation, which reasonably agrees with Köhler theory predictions of activation for both sea-salt aerosols and the various sulfate salts.

[39] The observations of *O'Dowd et al.* [1999] showed that because coarse mode sea salt will activate at very low supersaturations, it will draw water out of the vapor phase before higher supersaturations are reached. This lowers the maximum supersaturation reached in the cloud thus yielding a lower total number of activated cloud droplets than if the maximum supersaturation had remained the same. *Gong and Barrie* [2003] used this approach to determine cloud droplet number concentrations when they added sea salt to their sulfate model and found that including sea-salt aerosols reduced the cloud droplet number globally using this approach. In our case, we are looking to determine the error in CCN if sea salt is ignored when predicting stratiform clouds with a supersaturation of 0.2%. It remains for future work, with a more detailed parameterization of cloud-aerosol interaction, to determine the net effect of sea salt on cloud droplet number concentrations.

[40] Figures 9c–9f show the percentage increase in CCN(0.2%) concentrations from incorporating the four sea-salt parameterizations into TOMAS. The CLRK and MART simulations show the largest increases in CCN(0.2%) concentrations because they have the highest number flux below 500 nm. These values for global-average increases of CCN(0.2%) may overestimate the impact of sea salt because the model includes only sulfate and sea-salt aerosols. The potential underestimation of sulfate aerosol nucleation within the boundary layer due to reasons described in section 2.1 may also reduce the impact of sea salt on CCN(0.2%). However, areas such as the Southern Ocean may represent the impacts of sea salt on CCN(0.2%) more accurately because sea salt and sulfate are the dominant species and the large surface area provided by the sea-salt aerosols may suppress nucleation [*O'Dowd et al.*, 1997]. Also, the model's general bias towards lower sea-salt

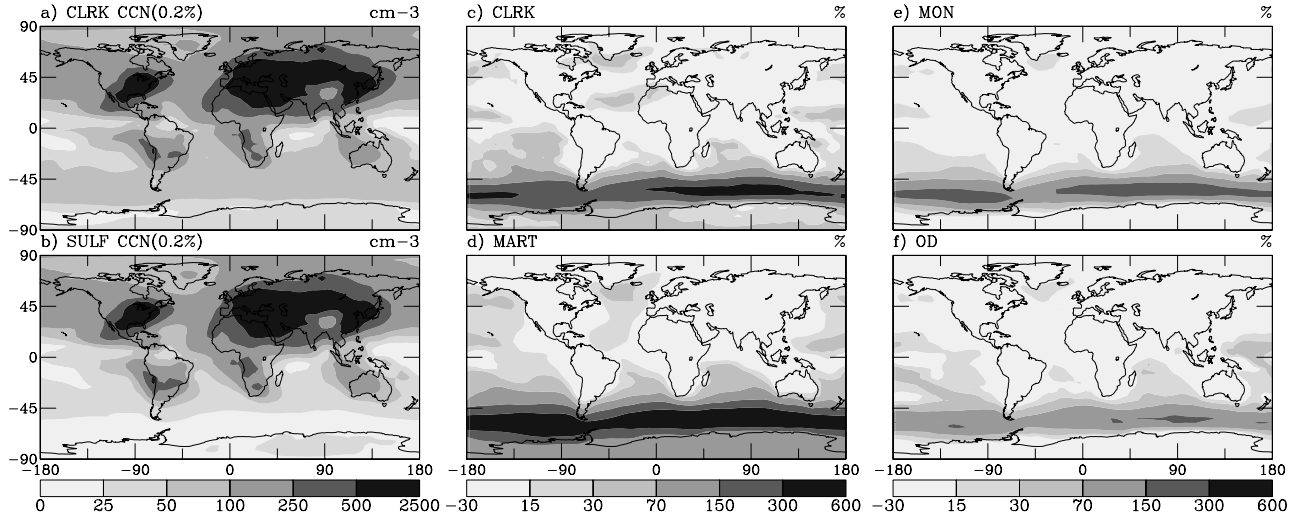

Figure 9. (a) Annual-average CCN(0.2%) concentrations [cm^{-3} at 273 K and 1 atm] in the model surface layer taken from CLRK simulation. (b) Same as Figure 9a, except taken from SULF run. (c) The percent change in CCN(0.2%) after adding Clarke sea-salt to sulfate-only model (CLRK versus SULF) [%]. (d) Same as Figure 9c, but MART versus SULF. (e) Same as Figure 9c, but MON versus SULF. (f) Same as Figure 9c, but OD versus SULF.

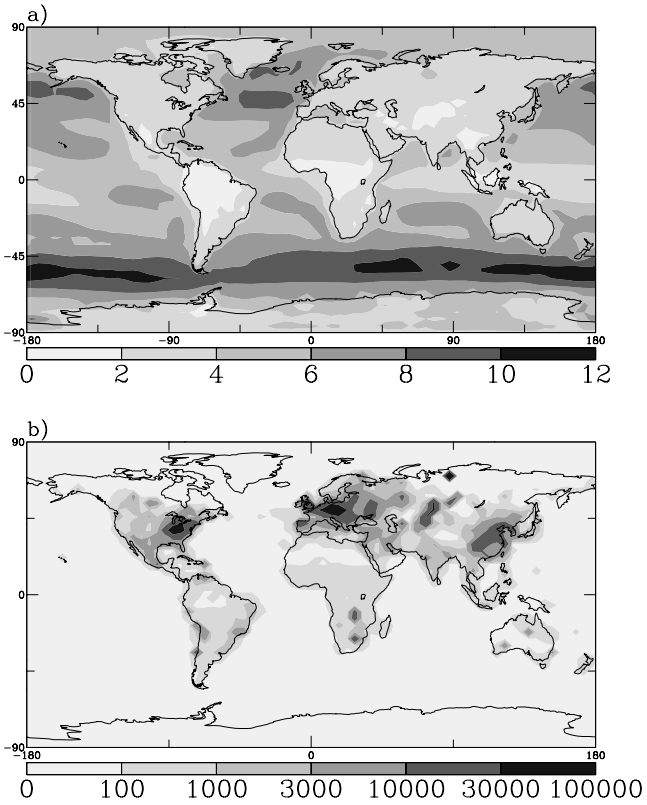

Figure 10. (a) Annual-average 10 m surface winds in the model for all simulations [ms^{-1}]. (b) Annual-average SO_2 emissions [10^{-14} kg m^{-2} s^{-1}].

emissions as discussed in section 2.3 may cause the impact of sea salt on CCN(0.2%) to be underpredicted.

[41] For all four sea-salt parameterizations, the largest percent increases in CCN(0.2%) concentrations are in oceanic areas with high winds and low continental influence. The CLRK and MART runs show greater than threefold increases in CCN(0.2%) concentrations in the Southern Ocean and more than 50% increases in some parts of the North Atlantic, North Pacific and subtropical Pacific and Indian Oceans. Figures 10a and 10b show the annual-average winds predicted by GISS II-prime and the annual-average SO_2 emissions. The Southern Ocean not only has the highest wind speeds but also very low continental influence, which can be seen both from Figure 9b and Figure 10b. The North Atlantic and North Pacific have much greater continental influence but have average wind speeds around 9 m s^{-1}, so the impact of sea salt on CCN(0.2%) is still relatively large. The subtropical Pacific and Indian Oceans have low continental influence and moderate winds that combine for a strong impact of sea salt.

[42] Over the Southern Ocean and Antarctica, the differences in predicted CCN(0.2%) concentrations between different simulations is significant. The average concentration in the lowest 3 km over the Southern Ocean (area average from 45–75 °S) in the MART simulation is about 80 cm^{-3}, whereas the average concentration for the OD run is about 40 cm^{-3}. A simple forcing calculation was done to estimate the order of magnitude of the resulting uncertainty in cloud forcing over this region. The change in cloud forcing, averaged over both clear and cloudy sky, can be estimated from the following equation [*Seinfeld and Pandis*, 1998];

$$\Delta F_C = -\frac{1}{3} F_0 A_C T_a^2 R_C (1 - R_C) \Delta \ln N \qquad (2)$$

In this equation, ΔF_C is the change in cloud forcing, F_0 is the incoming solar flux at the top of the atmosphere (218 W m^{-2} annual-average at 60°S), A_C is the fractional area covered by clouds (estimated as 0.6), T_a is the atmospheric transmittance (estimated as 0.76), R_C is the albedo of the cloud (0.6 for estimated cloud optical depth of 10), and N is the number concentration of CCN (varied from 40 to 80 cm^{-3}). This simple calculation gives an uncertainty in total cloud forcing of 4 W m^{-2} over this region as a sole result of different sea-salt emissions. While not a detailed estimate, this does show that differences in sea-salt parameterizations and resulting uncertainties in CCN concentrations could lead to uncertainties on the order of several W m^{-2} when calculating the natural cloud forcing over unpolluted regions with high wind speeds. Furthermore, this contributes to uncertainty in indirect effect predictions over polluted marine regions because the preindustrial marine CCN predictions will be sensitive to the sea-salt emissions similar to the remote marine atmosphere described here. This stresses the importance of accurate descriptions of sea-salt emissions, subsequent microphysical transformations and deposition lifetimes.

6. Ultrafine Sea Salt and CCN

[43] Because most previous sea-salt modeling studies have not included the ultrafine sea-salt emissions that were included in the CLRK and MART parameterizations, we have assessed their impact on CCN(0.2%) concentrations. Figure 11 shows the percent change in CCN(0.2%) concentrations from inclusion of ultrafine sea-salt particles versus omitting all sea-salt emissions below 0.1 μm. These figures show that the inclusion of ultrafine particles makes a large impact in remote regions especially in mid and high southern latitudes. The MART and MA100 simulations show a stronger influence of ultrafines than CLRK, even though their increases in CCN(0.2%) relative to the SULF model were more alike (see Figure 9). This results from the ultrafine particles being a high fraction of the sea salt emitted by the MART parameterization at low temperatures. Figure 2c shows the temperature dependence of the MART emissions. At cold temperatures, enough of the MART sea-salt number flux distribution occurs below 100 nm that omission of the ultrafine emissions cuts the CCN(0.2%) concentrations nearly in half. This is interesting considering the critical diameter for NaCl activation at 0.2% supersaturation is 80 nm, and the cutoff for the ultrafine particles is 100 nm. This implies that the size range between 80 and 100 nm dry diameter is the only range in which the ultrafines would activate at the sizes that they are emitted. The flux into this size range accounts for only a 40% increase in the emissions of particles large enough to be CCN(0.2%), yet the total number of CCN(0.2%) increases by over 60% at all latitudes south of 70°S (see Figure 11). Similarly for the CLRK run, the 80 to 100 nm size range accounts for

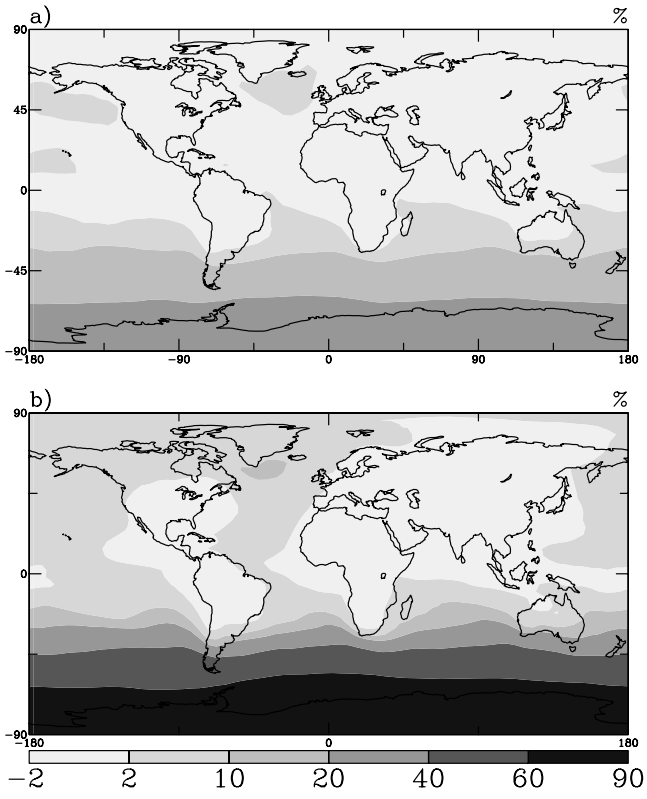

Figure 11. (a) Percent change in CCN(0.2%) after including ultrafine sea salt with the Clarke sea-salt parameterization (CLRK versus CL100). (b) Same as Figure 11a, but with Martensson parameterization (MART versus MA100).

only 15% of the total number emissions larger than 80 nm, but increases in CCN(0.2%) are as high as 40%. This implies that ultrafine sea-salt particles smaller than 80 nm are growing through condensation of sulfate, coagulation with other sub-80 nm particles, or some combination of these two processes. Examining the rates of condensation and coagulation in the latitudes over the Southern Ocean shows that condensation of sulfate is the dominant process for growth as coagulation of ultrafine particles occurs more readily with accumulation mode particles.

[44] The impact these ultrafine sea-salt emissions have on CCN depends greatly on the supersaturation of the cloud. At high supersaturations ($\sim$1%), ultrafine hydrophilic particles as small as 25 nm dry diameter may activate, making the CCN concentration even more sensitive to the ultrafine sea-salt emissions. At very low supersaturations (<0.1%), the emissions of ultrafine sea salt may not have a large effect on the CCN concentration, even over the Southern Ocean and Antarctica.

[45] The addition of ultrafine sea-salt emissions brings additional uncertainty to cloud radiative forcings in areas where sea salt is the dominant aerosol species. The variability in CCN(0.2%) between the simulations with and without ultrafine sea salt was estimated to have an area-averaged cloud forcing on the order of $\sim$1 W m^{-2} over the Southern Ocean by using the same technique used in the previous section. This uncertainty is included in the uncertainty discussed in the last section because the parameterizations with the highest CCN(0.2%) concentrations over the Southern Ocean included emissions of ultrafine sea salt.

7. Conclusions

[46] Global simulations of sulfate and sea-salt aerosols with the detailed size-resolved microphysics of the TOMAS algorithm were performed in the GISS II-prime general circulation model. Four different sea-salt parameterizations were used in corresponding model runs. When compared to monthly averaged measurements of total sea-salt aerosol mass concentrations at several sampling stations, results from simulations using the four parameterizations compared differently due to differences in the treatment of supermicron aerosols between the parameterizations. In general, the OD and CLRK (see Table 1) simulations had the smallest errors. The CLRK simulation most closely matched the sea-salt mass distribution and the MART simulation performed best in the marine aerosol number distribution comparison. However, it was shown in section 2.3 that our model sea-salt emissions are biased low compared to NCEP reanalyzed wind fields and in section 3 that budget properties are not consistent between models. Therefore, firm conclusions regarding the accuracy of the emissions parameterizations themselves are difficult to obtain by comparing model predictions to observations. Such an evaluation, at the very least, would require carefully constraining the host meteorological model's wind speeds to observed values for the time period in question.

[47] Incorporating sea-salt emissions into the model increases the concentrations of CCN(0.2%) over most remote oceanic areas. The largest percentage increases occurred in areas with low continental influence and high wind speeds. The CLRK and MART simulations showed the greatest relative increases in CCN(0.2%) concentrations, with increases as high as 500% in the Southern Ocean. The increases in CCN(0.2%) concentrations for the CLRK and MART simulations are 2–3 times greater globally than the MON and OD runs.

[48] Including ultrafine sea-salt emissions had a large impact on the CCN(0.2%) concentrations in remote regions of the atmosphere. The inclusion of ultrafine sea salt into the MART model run caused CCN(0.2%) to increase by as much as 80% over Antarctica and 60% over much of the Southern Ocean. Much of these increases resulted from condensation of sulfate onto sub-80 nm particles allowing them to grow to CCN(0.2%) sizes. Due to different fluxes of ultrafine particles, the sensitivity to the inclusion of ultrafine emissions in the MART simulation was about double that of the CLRK even though the parameterizations' overall impacts on CCN(0.2%) were similar. At higher supersaturations, more of the ultrafine particles will activate increasing the importance of ultrafine sea-salt emissions.

[49] The analysis of ultrafine sea-salt aerosols shows that, if in fact ultrafine sea-salt emissions are as large as those predicted by the CLRK and MART parameterizations, they may have a substantial impact on CCN concentrations in remote oceanic areas and neighboring continental areas. In this model, the ultrafine sea-salt emissions of CLRK and MART simulations were necessary to explain the ultrafine number concentrations in the area around the Southern

Ocean (see Figure 8 and Table 4). This sensitivity to ultrafine sea-salt emissions shows that, in order to develop accurate global CCN models to assess the indirect effect of aerosols on climate, both the ultrafine and accumulation mode sea-salt emissions must be parameterized properly. Currently, there is a large variability in the shape and magnitude of the sea-salt emissions distribution functions (see Figure 2). Furthermore, the effect of temperature on the sea-salt size distribution has been incorporated into the MART source function but not into other parameterizations. The temperature dependence had a strong impact on CCN(0.2%) in different parts of the world by increasing ultrafine emissions and decreasing coarse emissions in regions with colder ocean temperatures. This temperature dependence needs to be explored further. Also, giant sea-salt particles ($D_p > 10$ μm), not yet included in this model, may play an important role in controlling the maximum supersaturations reached in a cloud, and therefore the CCN concentrations. As the scientific community refines these emissions functions, the uncertainty associated with sea-salt aerosols and CCN could be greatly reduced.

[50] **Acknowledgments.** The authors thank Antony Clarke for providing us with his sea-salt emissions parameterization prior to its publication. NCEP Reanalysis data were provided by the NOAA-CIRES Climate Diagnostics Center, Boulder, Colorado, USA, from their Web site at http://www.cdc.noaa.gov/. This research was supported by the United States National Aeronautics and Space Administration through grant RSP-0153-0289.

References

Adams, P. J., and J. H. Seinfeld (2002), Predicting global aerosol size distributions in general circulation models, *J. Geophys. Res.*, *107*(D19), 4370, doi:10.1029/2001JD001010.

Adams, P. J., and J. H. Seinfeld (2003), Disproportionate impact of particulate emissions on global cloud condensation nuclei concentrations, *Geophys. Res. Lett.*, *30*(5), 1239, doi:10.1029/2002GL016303.

Albrecht, B. A. (1989), Aerosols, cloud microphysics, and fractional cloudiness, *Science*, *245*, 1227–1230.

Andreae, M. O., W. Elbert, Y. Cai, T. W. Andreae, and J. Gras (1999), Non-sea-salt sulfate, methanesulfonate, and nitrate aerosol concentrations and size distributions at Cape Grim, Tasmania, *J. Geophys. Res.*, *104*, 21,695–21,706.

Andreas, E. L. (1998), A new sea spray generation function for wind speeds up to 32 m s^{-1}, *J. Phys. Oceanogr.*, *28*, 2175–2184.

Angstrom, A. (1929), On the atmospheric transmission of sun radiation and on dust in the air, *Geogr. Ann.*, *11*, 156–166.

Boucher, O., and U. Lohmann (1995), The sulfate-CCN-cloud albedo effect, *Tellus*, *47B*, 281–300.

Cakmur, R. V., R. L. Miller, and O. Torres (2004), Incorporating the effect of small-scale circulations upon dust emission in an atmospheric general circulation model, *J. Geophys. Res.*, *109*, D07201, doi:10.1029/2003JD004067.

Charlson, R. J., S. E. Schwartz, J. M. Hales, R. D. Cess, J. A. Coakley, J. E. Hansen, and D. J. Hofman (1992), Climate forcing by anthropogenic aerosols, *Science*, *255*, 423–430.

Chuang, C. C., and J. E. Penner (1995), Effects of anthropogenic sulfate on cloud drop nucleation and optical-properties, *Tellus*, *47*, 566–577.

Chuang, C. C., J. E. Penner, K. E. Taylor, A. S. Grossman, and J. J. Walton (1997), An assessment of the radiative effects of anthropogenic sulfate, *J. Geophys. Res.*, *102*, 3761–3778.

Clarke, A. D., et al. (1998), Particle nucleation in the tropical boundary layer and its coupling to marine sulfur sources, *Science*, *282*, 89–92.

Clarke, A. D., S. R. Owens, and J. Zhou (2006), An ultrafine sea-salt flux from breaking waves: Implications for CCN in the remote marine atmosphere, *J. Geophys. Res.*, *111*, D06202, doi:10.1029/2005JD006565.

Del Genio, A. D., and M.-S. Yao (1992), Efficient cumulus parameterization for long-term climate studies: The GISS scheme, *Meteorol. Monogr.*, *24*, 181–184.

Del Genio, A. D., M.-S. Yao, W. Kovari, and K. Lo (1996), A prognostic cloud water parameterization for global models, *J. Clim.*, *9*, 270–304.

Feingold, G., S. Tzivion, and Z. Levin (1988), Evolution of raindrop spectra. Part I: Solution to the stochastic collection/breakup equation using the method of moments, *J. Atmos. Sci.*, *45*, 3387–3399.

Feingold, G., W. R. Cotton, S. M. Kreidenweis, and J. T. Davis (1999), The impact of giant cloud condensation nuclei on drizzle formation in stratocumulus: Implication for cloud radiative properties, *J. Atmos. Sci.*, *56*, 4100–4117.

Ghan, S., R. Easter, J. Hudson, and F. M. Breon (2001), Evaluation of aerosol indirect radiative forcing in MIRAGE, *J. Geophys. Res.*, *106*, 5317–5334.

Gong, S. L. (2003), A parameterization of sea-salt aerosol source function for sub- and super-micron particles, *Global Biogeochem. Cycles*, *17*(4), 1097, doi:10.1029/2003GB002079.

Gong, S. L., and L. A. Barrie (2003), Simulating the impact of sea salt on global nss sulphate aerosols, *J. Geophys. Res.*, *108*(D16), 4516, doi:10.1029/2002JD003181.

Gong, S. L., L. A. Barrie, and J. P. Blanchet (1997), Modeling sea-salt aerosols in the atmosphere: 1. Model development, *J. Geophys. Res.*, *102*, 3805–3818.

Gong, S. L., L. A. Barrie, and M. Lazare (2002), Canadian Aerosol Model (CAM): A size-segregated simulation of atmospheric aerosol processes for climate and air quality models: 2. Global sea-salt aerosol and its budgets, *J. Geophys. Res.*, *107*(D24), 4779, doi:10.1029/2001JD002004.

Gong, S. L., et al. (2003), Canadian Aerosol Module: A size-segregated simulation of atmospheric aerosol processes for climate and air quality models: 1. Module development, *J. Geophys. Res.*, *108*(D1), 4007, doi:10.1029/2001JD002002.

Grini, A., G. Myhre, J. K. Sundet, and I. S. Isaksen (2002), Modeling the annual cycle of sea salt in the global 3D model Oslo CTM2: Concentrations, fluxes and radiative impact, *J. Clim.*, *15*, 1717–1730.

Guelle, W., M. Schulz, and Y. Balkanski (2001), Influence of the source formulation on modeling the atmospheric global distribution of sea salt aerosol, *J. Geophys. Res.*, *106*, 27,509–27,524.

Hansen, J., G. Russell, D. Rind, P. Stone, A. Lacis, S. Lebedeff, R. Ruedy, and L. Travis (1983), Efficient 3-dimensional global-models for climate studies - Model-I and Model-II, *Mon. Weather Rev.*, *111*, 609–662.

Hartke, G. J., and D. Rind (1997), Improved surface and boundary layer models for the Goddard Institute for Space Studies general circulation model, *J. Geophys. Res.*, *102*, 16,407–16,422.

Heintzenberg, J., D. C. Covert, and R. V. Van Dingenen (2000), Size distribution and chemical composition of marine aerosols: A compilation and review, *Tellus*, *52B*, 1104–1122.

Herzog, M., D. K. Weisenstein, and J. E. Penner (2004), A dynamic aerosol module for global chemical transport models: Model description, *J. Geophys. Res.*, *109*, D18202, doi:10.1029/2003JD004405.

Howell, S., A. A. P. Pszenny, P. Quinn, and B. Huebert (1998), A field intercomparison of three cascade impactors, *Aerosol Sci. Technol.*, *29*, 475–492.

Intergovernmental Panel on Climate Change (IPCC) (2001), The scientific basis—Technical summary, Geneva.

Jacobson, M. Z. (2002), Analysis of aerosol interactions with numerical techniques for solving coagulation, nucleation, condensation, dissolution, and reversible chemistry among multiple size distributions, *J. Geophys. Res.*, *107*(D19), 4366, doi:10.1029/2001JD002044.

Kettle, A. J., et al. (1999), A global database of sea surface dimethylsulfide (DMS) measurements and a procedure to predict sea surface DMS as a function of latitude, longitude, and month, *Global Biogeochem. Cycles*, *13*, 399–444.

Koch, D., D. Jacob, I. Tegen, D. Rind, and M. Chin (1999), Tropospheric sulfur simulation and sulfate direct radiative forcing in the Goddard Institute for Space Studies general circulation model, *J. Geophys. Res.*, *104*, 23,799–23,822.

Lewis, E. R., and S. E. Schwartz (2004), *Sea-Salt Aerosol Production: Mechanisms, Methods, Measurements, and Models—A Critical Review*, 412 pp., AGU, Washington, D. C.

Liao, H., J. H. Seinfeld, P. J. Adams, and L. J. Mickley (2004), Global radiative forcing of coupled tropospheric ozone and aerosols in a unified general circulation model, *J. Geophys. Res.*, *109*, D16207, doi:10.1029/2003JD004456.

Liss, P. S., and L. Merlivat (1986), Air-sea gas exchange rates: Introduction and synthesis, in *The Role of Air-Sea Exchange in Geochemical Cycling*, pp. 113–127, Springer, New York.

Martensson, E. M., E. D. Nilsson, G. de Leeuw, L. H. Cohen, and H.-C. Hansson (2003), Laboratory simulations and parameterizations of the primary marine aerosol productions, *J. Geophys. Res.*, *108*(D9), 4297, doi:10.1029/2002JD002263.

Monahan, E. C., and I. O'Muircheartaigh (1980), Optimal power-law description of oceanic whitecap coverage dependence on wind speed, *J. Phys. Oceanogr.*, *10*, 2094–2099.

Monahan, E. C., D. E. Spiel, and K. L. Davidson (1986), A model of marine aerosol generation via whitecaps and wave disruption, *Oceanic Whitecaps*, 167–174.

O'Dowd, C. D., M. H. Smith, I. E. Consterdine, and J. A. Lowe (1997), Marine aerosol, sea salt, and the marine sulpher cycle: A short review, *Atmos. Environ.*, *31*, 73–80.

O'Dowd, C. D., J. A. Lowe, M. H. Smith, and A. D. Kaye (1999), The relative importance of non-sea-salt sulfate and sea-salt aerosol to the marine cloud condensation nuclei population: An improved multi-component aerosol-cloud droplet parameterization, *Q. J. R. Meteorol. Soc.*, *125*, 1295–1313.

Prather, M. J. (1986), Numerical advection by conservation of second-order moments, *J. Geophys. Res.*, *91*, 6671–6681.

Quinn, P. K., and D. J. Coffman (1999), Comment on "Contribution of different aerosol species to the global aerosol extinction optical thickness: Estimates of model results" by Tegan et al., *J. Geophys. Res.*, *104*, 4241–4248.

Rind, D., and J. Lerner (1996), Use of on-line tracers as a diagnostic tool in general circulation model development: 1. Horizontal and vertical transport in the troposphere, *J. Geophys. Res.*, *101*, 12,667–12,683.

Rodriguez, M. A., and D. Dabdub (2004), IMAGES-SCAPE2: A modeling study of size- and chemically resolved aerosol thermodynamics in a global chemical transport model, *J. Geophys. Res.*, *109*, D02203, doi:10.1029/2003JD003639.

Savoie, D. L., and J. M. Prospero (1977), Aerosol concentration statistics for northern tropical Atlantic, *J. Geophys. Res.*, *82*, 5954–5964.

Seinfeld, J. H., and S. N. Pandis (1998), *Atmospheric Chemistry and Physics*, John Wiley, Hoboken, N. J.

Smith, M. H., P. M. Park, and I. E. Consterdine (1993), Marine aerosol concentration and estimated fluxes over the sea, *Q. J. R. Meteorol. Soc.*, *119*, 809–824.

Stier, P., et al. (2005), The aerosol-climate model ECHAM5-HAM, *Atmos. Chem. Phys.*, *5*, 1125–1156.

Twomey, S. (1974), Pollution and the planetary albedo, *Atmos. Environ.*, *8*, 1251–1256.

Twomey, S. (1977), The influence of pollution on the shortwave albedo of clouds, *J. Atmos. Sci.*, *34*, 1149–1152.

Tzivion, S., G. Fiengold, and Z. Levin (1987), An efficient numerical solution to the stochastic collection equation, *J. Atmos. Sci.*, *44*, 3139–3149.

Vignati, E., J. Wilson, and P. Stier (2004), M7: An efficient size-resolved aerosol microphysics module for large-scale aerosol transport models, *J. Geophys. Res.*, *109*, D22202, doi:10.1029/2003JD004485.

Wilson, J., C. Cuvelier, and F. Raes (2001), A modeling study of global mixed aerosol fields, *J. Geophys. Res.*, *106*, 34,081–34,108.

P. J. Adams, Department of Civil and Environmental Engineering, Carnegie Mellon University, Pittsburgh, PA 15213, USA.

J. R. Pierce, Department of Chemical Engineering, Carnegie Mellon University, Pittsburgh, PA 15213, USA. (jrpierce@andrew.cmu.edu)